JOURNAL OF SOLID STATE CHEMISTRY **134,** 192–197 (1997)
ARTICLE NO. SC977576

$Zn_{2-x}Sn_{1-x}In_{2x}O_{4-\delta}$: An Indium-Substituted Spinel with Transparent Conducting Properties

G. B. Palmer[1] and K. R. Poeppelmeier[2]

Department of Chemistry and Materials Research Center, Northwestern University, Evanston, Illinois 60208-3113

and

T. O. Mason[3]

Department of Materials Science and Engineering and Materials Research Center, Northwestern University, Evanston, Illinois 60208

Received May 1, 1997; accepted July 29, 1997

A substantial solid solubility of In_2O_3 in the spinel Zn_2SnO_4 ($Zn_{2-x}Sn_{1-x}In_xO_{4-\delta}$, $x = 0$ to 0.45) was discovered. The reduced material showed improved conductivity at higher In contents.

INTRODUCTION

Transparent conducting oxides (TCO's) have widespread uses as electrodes in solar cells and liquid crystal displays and as heat-reflecting window coatings. The commercial TCO of choice is ITO (tin-doped indium oxide). ITO has a typical conductivity of $1 - 5 \times 10^3$ S/cm and a transparency 85–90% in thin films (1).

In addition to ITO, which has been reviewed (2), a number of promising TCO's consisting of various oxide combinations of In, Sn, and Zn have been reported (3–6). In particular, several zinc-stannate TCO's have been reported. Enoki *et al.* (7) produced Zn_2SnO_4 thin films and observed 80% transparency, a 3.20 eV band gap, and conductivities of 20 S/cm (as prepared) and 59 S/cm (reduced). In ZnO-substituted Cd_2SnO_4 films, Enoki *et al.* (8) observed worse conductivity and larger band gap as the Zn content increased. Minami *et al.* (9) produced an amorphous, reduced, zinc-stannate film with 200 S/cm conductivity. They suggested that the parent structure was $ZnSnO_3$, although the zinc content of the film was less than 33 cation %. Palmer *et al.* (10) investigated ZnO/SnO_2-cosubstituted In_2O_3 ($In_{2-2x}Sn_xZn_xO_{3-\delta}$) and found a conductivity of 2500 S/cm in a 90% In sample, but observed decreasing conductivity as In% was lowered.

[1] E-mail: g-palmer@nwu.edu.
[2] E-mail: krp@nwu.edu.
[3] E-mail: t-mason@nwu.edu.

Nonequilibrium conditions may exist in thin-film deposition. However, knowledge of equilibrium phase relationships and physical properties of bulk phases can assist interpretation of existing film materials and direct the synthesis of new film materials. In this article, we present the phase relations and physical properties of In_2O_3-substituted Zn_2SnO_4: $Zn_{2-x}Sn_{1-x}In_{2x}O_{4-\delta}$.

Zn_2SnO_4 (JCPDS Card No. 6-416) is a $+2/+4$, inverse spinel (11). The unit cell is face-centered cubic (space group $Fd\bar{3}m$) with lattice parameter, $a = 8.6574$. All Sn^{4+} are octahedrally coordinated. Zn^{2+} are distributed half in tetrahedral coordination, half in octahedral coordination.

EXPERIMENTAL

Synthesis

Sample compositions are shown in Table 1. In addition to compositions along the join between Zn_2SnO_4 and $Zn_{2-x}Sn_{1-x}In_{2x}O_{4-\delta}$, samples along the Zn_2SnO_4–ZnO and Zn_2SnO_4–SnO_2 joins were made. Powders were prepared from 99.99% In_2O_3, 99.9% SnO_2, and 99.99% ZnO powders (cation basis, Aldrich). Samples were ground together under acetone with an agate mortar and pestle. Pellets were uniaxially pressed in a steel die at 51.7 MPa (Carver 3392 Laboratory Press). Sample pellets were fired in alumina crucibles. The pellets were buried in their constituent powders to minimize reaction with the alumina crucibles or evaporation of the metal oxides. Samples were initially heated at 1100°C for 4 days. The samples were then removed, reground, and repelletized prior to a final heating at 1250°C for 3 days. Mass losses averaged 0.4% for the 1100°C firing and 1.5% for the 1250°C firing.

Samples were quenched by removing the sample crucibles from the at-temperature furnace and inverting them over a copper plate which served as a nonreactive heat sink. To

0022-4596/97 $25.00

TABLE 1
Sample Compositions and Colors

x	% $InO_{1.5}$	% SnO_2	% ZnO	Color (unreduced)	Color (reduced)
0	100	0	0	white	white
0.05	3.33	31.67	65	white	gray
0.1	6.67	30	63.33	white	gray, darker than $x = 0.05$
0.15	10.0	28.33	61.67	white	gray, darker than $x = 0.1$
0.2	13.33	26.67	60	white	gray, darker than $x = 0.15$
0.25	16.67	25	58.33	white	gray, darker than $x = 0.2$
0.30	20.0	23.33	56.67	white (faint gray–green)	NA
0.45	30.0	18.33	51.67	lime green–gray	NA
0.60[a]	40.0	13.33	46.67	light green–gray	NA
NA	0	5	95	light jade gray–green	NA
NA	0	20	80	light yellow	NA
NA	0	66.7	33.3	white	NA
NA	0	90	10	white	NA

[a] Theoretical value, solubility extends to $x = 0.45$.

accelerate quenching, the glowing pellets and powders were moved rapidly over the copper plate and were at room temperature within a few seconds. Visual inspection of the copper plate and sample pellets showed no copper melting or copper reaction with the pellets.

Selected samples were reduced in flowing 7% H_2/93% N_2. An initial reduction was performed at 400°C for 1 h and a subsequent reduction at 500°C for 12 h.

X-Ray Crystallography

Powder X-ray diffraction was used to determine phase composition after both firings (Rigaku). Copper $K\alpha$ radiation was used at 40 kV and 20 mA. LiF (JCPDS Card No. 4-857, Copper $K\alpha 1$) was used as an internal X-ray standard after shifting the peaks to correspond to (mixed) $K\alpha$ radiation. The average shift of the observed LiF peaks was used to make an off-axis correction (two-theta shift) to the observed sample peaks. X-ray peaks were fitted using XRAYFIT (12), and lattice constants were calculated with a least-squares averaging program, POLSQ (13).

Electronic Measurements

Room temperature electrical conductivities of as-fired pellets were measured with a spring-loaded linear four-probe apparatus. Applied currents ranged from 0.01 to 1 mA (Model 225, Keithly Current Source). Voltages were measured with a voltmeter (Model 197, Keithly). The conductivity was calculated as

$$\sigma = \frac{1}{\rho} = \frac{1}{\frac{V}{I} wC\left(\frac{d}{s}\right) F\left(\frac{w}{s}\right)},$$

where σ is conductivity, ρ is resistivity, V is measured voltage, I is excitation current, w is width, d is diameter, s is electrode spacing, and $C(d/s)$ and $F(w/s)$ are correction factors for sample geometry and finite thickness, respectively (14). To ensure meaningful comparisons, conductivities were divided by percent theoretical density, which roughly doubled the measured conductivities.

Optical Measurements

Diffuse reflectance was used to determine the relative optical transmission of the bulk samples in this study (15). The diffuse reflectance of as-fired pellets was measured from 190 to 800 nm using a double-beam spectrophotometer with integrating sphere (Cary 1E with Cary 1/3 attachment, Varian). A pressed PTFE powder compact (Varian part number 04-101439-00) was used as a high-transmission reference. A blackened sample mask was used to mount pellet samples. A background scan with the sample mask was performed and subtracted from all spectra. To limit specular reflectance, as-fired pellets were used with no surface polishing. After diffuse reflectance, the pellet internals were compared visually to the exterior surfaces, with no color differences noted.

RESULTS AND DISCUSSION

Appearance and Morphology

After firing, all pellets were sintered into semihard pellets. Theoretical densities were calculated from observed lattice parameters and starting mixture stoichiometry. Actual pellet densities were calculated directly from pellet mass and dimensions. Densities averaged 55% of theoretical.

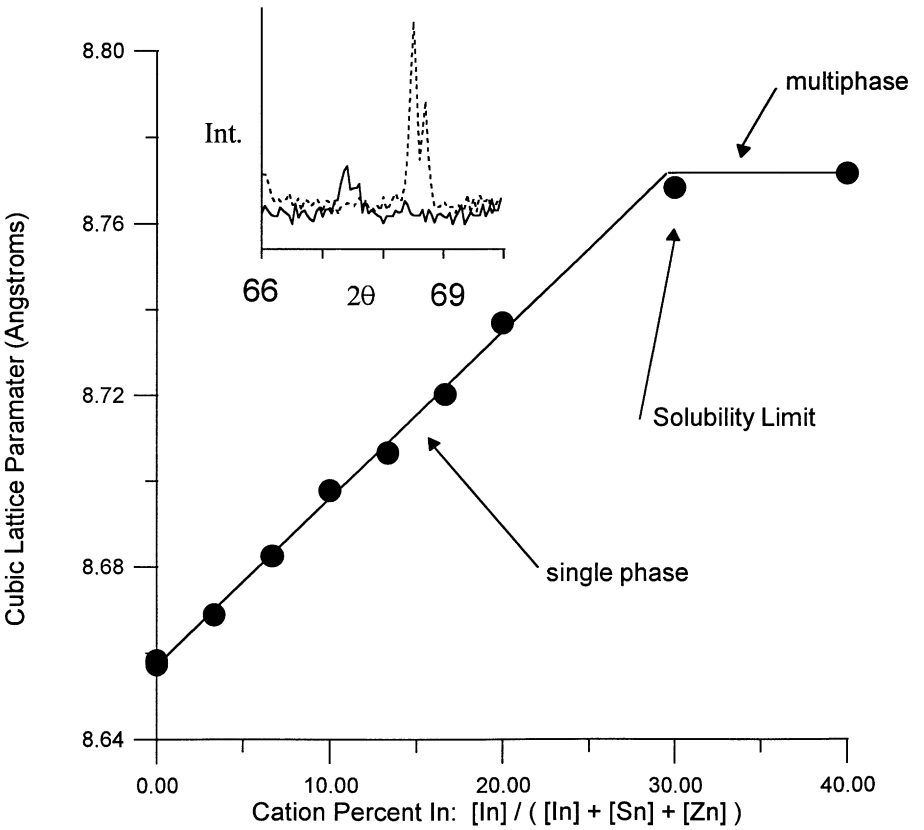

FIG. 1. Plot of lattice parameter versus substitution extent (expressed as In cation %). The sloping region is single-phase. The horizontal line is three-phase. The inset graphic shows the pronounced two-theta shift observed in the powder patterns between the pure spinel sample (dashed line) and the 30% In-substituted spinel (solid line).

Pellet colors are summarized in Table 1. After the 1250°C heating, the substituted spinel samples were white from 0 to 20% In. After reduction, these samples were all slightly gray except for the Zn_2SnO_4 sample, which remained white. The samples were progressively darker, as In content increased. Samples along the Zn_2SnO_4–SnO_2 join were white regardless of composition, while those along the Zn_2SnO_4–ZnO join were darker with increasing Zn content.

Crystal Structure and Phase Equilibria

Figure 1 shows the change in cubic lattice parameter a with In substitution of $Zn_{2-x}Sn_{1-x}In_{2x}O_{4-\delta}$. The inset graphic shows the 620 peak of $x = 0$ and $x = 0.45$ samples. As x increases, the X-ray reflections shift to lower values, indicating a larger unit cell. The lattice parameter shift follows Vegard's Rule in the solid solution region with a 0.9953 linear correlation coefficient (r factor). The larger lattice parameter of the indium-substituted spinel is reasonable based on the ionic radii sizes of the metal cations. In^{3+} (0.800 Å) has a larger 6-coordinate ionic radii than either Zn^{2+} (0.740 Å) or Sn^{4+} (0.690) (16). From Fig. 1, the solubility limit is 30% In.

In contrast to $Zn_{2-x}Sn_{1-x}In_{2x}O_{4-\delta}$, Zn_2SnO_4 showed minimal solubilities of ZnO or SnO_2 based on lattice parameter shifts. The average lattice constants of pure spinel, ZnO-saturated spinel, and SnO_2-saturated spinel were 8.658, 8.658, and 8.663 Å, respectively.

With In_2O_3 substitution, a Sn^{4+}/Zn^{2+} pair is removed for every two In^{3+} added to the structure. The result is an overall *iso*valent substitution that explains the dramatic solubility. This result can be thought of as a reverse of the large cosolubility of ZnO and SnO_2 into In_2O_3 (10). The initial intention was to determine how close one could get to complete substitution of In_2O_3 into Zn_2SnO_4 (to form the spinel $ZnIn_2O_4$). This would be similar to the Zn_2SnO_4–$ZnFe_2O_4$ system, which forms a complete solid solution at 1060°C (17).

Phillips *et al.* claimed $ZnIn_2O_4$ was a "known stable spinel structure material," and might be the parent structure for their amorphous $ZnIn_{1.7}Sn_{0.3}O_{4.15-\delta}$ TCO film (5). A literature search showed no evidence for a spinel in the Zn–In oxide system (6, 18–20). Moreover, at 1250°C,

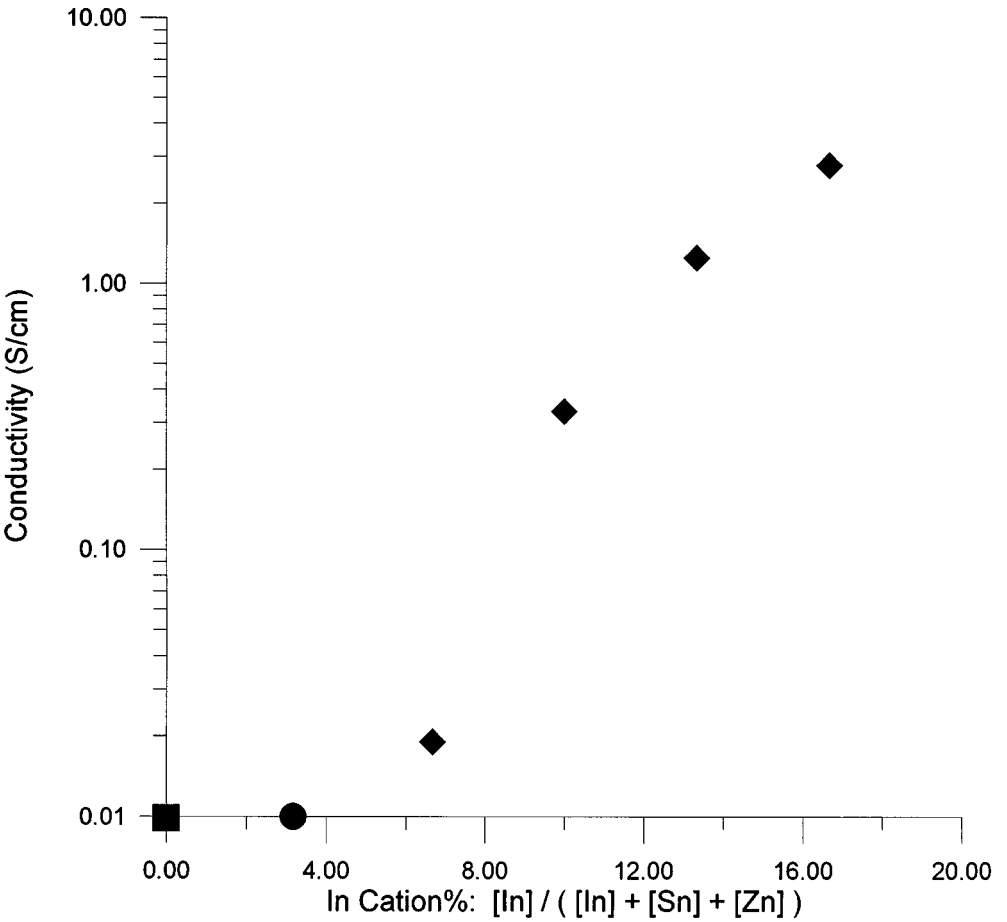

FIG. 2. Plot of conductivity versus cosubstitution extent (% In). The 0% In sample (■) had off-scale low conductivity, less than 4×10^{-6} S/cm. The 3.33% In sample (●) showed higher conductivity as evidenced by sporadic (nonpolarity reversible) voltage readings. The higher In content samples (◆) showed measurable conductivity readings as indicated.

the limit for In content in the Zn_2SnO_4 spinel is $Zn_{1.55}In_{0.9}Sn_{0.55}O_{4-\delta}$. While we recognize that thin film equilibria may differ from bulk equilibria, our study suggests that the amorphous film (by X-ray) of Phillips *et al.* may have contained spinel as an impurity phase. Thin-film microstructures in the Zn–Sn–In–O system should be inves tigated in light of the present results for bulk materials.

Previous structure determinations with direct calculation of intensities have shown that Zn_2SnO_4 is an inverse spinel but have not supplied an *R* factor (11, 21). A FULLPROF (22) Reitveld analysis (8% *R* factor) for this study agreed with earlier structure determinations.

Electronic Properties

The as-prepared $Zn_{2-x}Sn_{1-x}In_{2x}O_{4-\delta}$ samples with In% = 3.33, 6.67, 10, 13.33, and 16.67 were measured on the four-probe apparatus and exhibited conductivities too low to be measured. Considering the instrument off-scale setpoint, these conductivities were estimated to be less than 4×10^{-6} S/cm. After the first, mild reduction, conductivities were still too small to be measured for these samples and for a pure spinel sample. After the second, harsh reduction, conductivities were obtained as shown in Fig. 2. The improvement of conductivity by reduction is consistent with observations in similar In–Sn–Zn oxide TCO's (6). It is also evident from the figure that increasing In content correlated with higher conductivity. To ensure meaningful comparisons, sample reductions were carried out under the same conditions, i.e., simultaneously in the same furnace.

Optical Properties

The optical band gap was estimated as roughly equal to the transmission (diffuse reflectance) onset. Figure 3 shows optical band gaps of as-prepared and reduced (second reduction) samples. Comparison of reduced and unreduced samples indicates a noticeable band gap widening

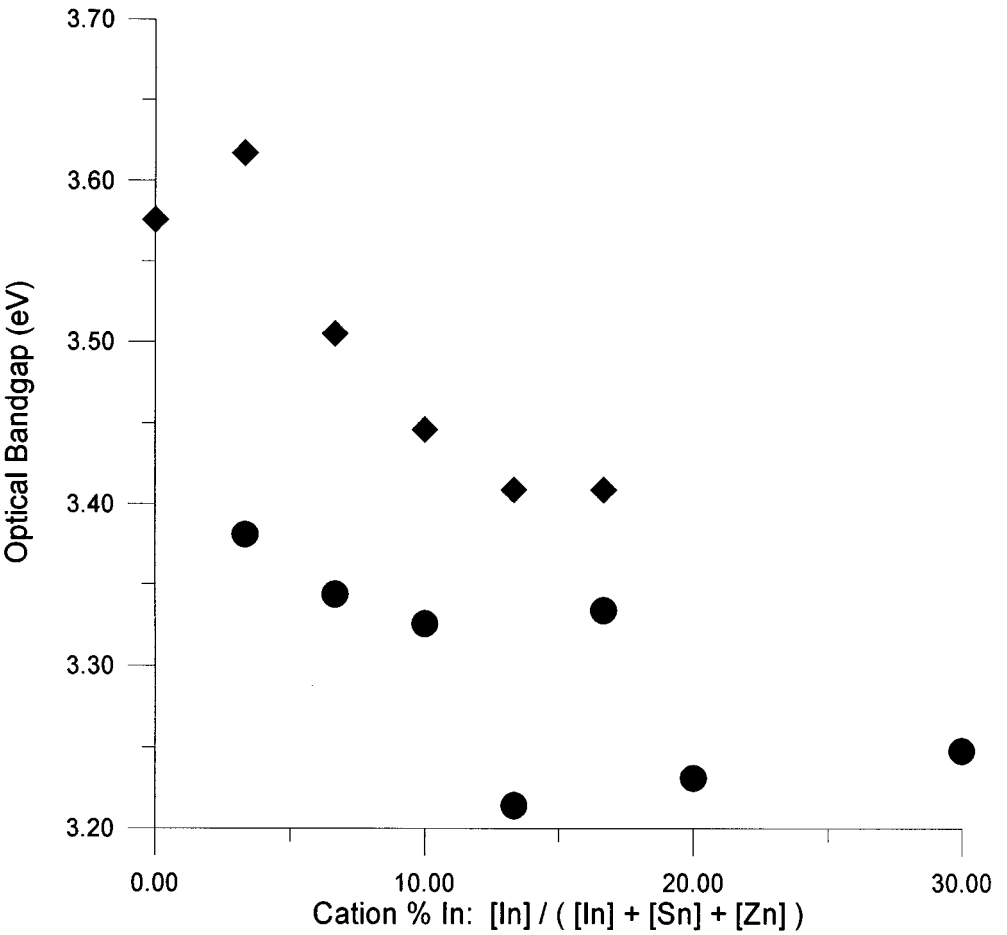

FIG. 3. Plot of optical band gap versus % In: as-fired (●) and reduced (◆) samples.

(Moss–Burstein (23) shift). It is also apparent that, independent of reduction, increased In correlates with band gap narrowing. Figure 4 shows the peak (500 nm) percentage of transmission for reduced and unreduced samples. As expected based on the visible color changes (see Table 1), the reduced samples had significantly lower peak visible light transmissions. Also consistent with the observed colors, rising In content in both data sets correlated with lower peak transmission.

CONCLUSION

Solid-state processing techniques and X-ray diffraction have been used to examine phase equilibria of Zn_2SnO_4 and ZnO, SnO_2, and In_2O_3. Study of bulk material has allowed relative comparisons of physical properties in stoichiometrically controlled TCO's. Pure Zn_2SnO_4 has been shown to have very low conductivity, even after strong reduction. Zn_2SnO_4 has negligible solid solubility of SnO_2 or ZnO. Since both SnO_2 and ZnO are known TCO's, the phase composition of zinc-stannate thin films should be carefully examined to determine the cause of observed physical properties, especially conduction.

The conductivity of Zn_2SnO_4 can be improved by incorporation of In^{3+} cations and subsequent reduction. In^{3+} is a net isovalent dopant (two In^{3+} added for every one Zn^{2+} and one Sn^{4+} removed). Thus, as-prepared $Zn_{2-x}Sn_{1-x}In_{2x}O_4$ shows similar poor conductivity to Zn_2SnO_4. However, after reduction, $Zn_{2-x}Sn_{1-x}In_{2x}O_{4-\delta}$ shows improved conductivity correlating to In substitution. Presumably the substituted material stabilizes oxygen vacancy donors. It is not known whether this is because of the larger lattice in the substituted spinel or because In^{3+} cations directly stabilize oxygen vacancies.

ACKNOWLEDGMENTS

This work was supported by the MRSEC program of the National Science Foundation (DMR-9632472) at Northwestern University and made use of the Central Facilities of the MRSEC program. George Palmer

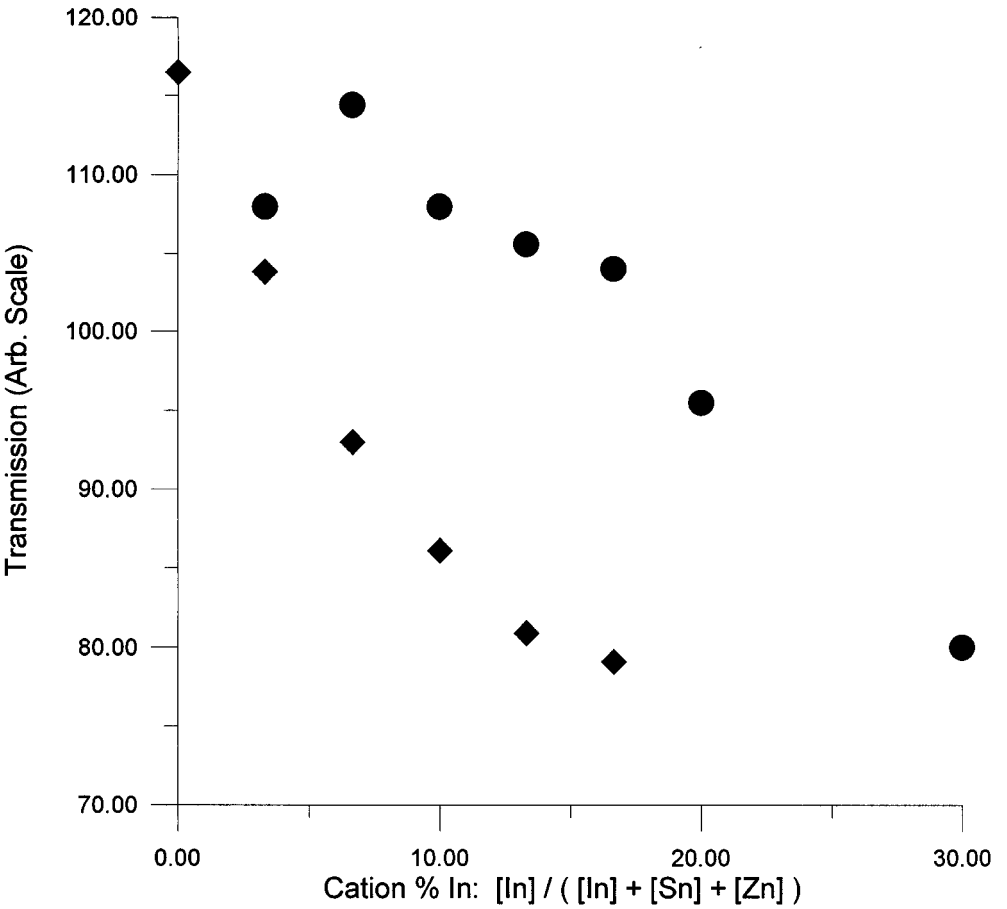

FIG. 4. Plot of peak (500 nm) transmittance versus % In: as-fired (●) and reduced (◆) samples.

was supported by a National Defense Science and Engineering Graduate fellowship funded by the Office of Naval Research. Professor Carl Kannewurf and Dr. Jon Schindler provided the use of and training on the four-probe apparatus.

REFERENCES

. 1. N. R. Lyman, *Proceedings of the symposium on electrochromic materials*, *Electrochem. Soc. Proc.* **90–92,** 201 (1990).
2. I. Hamberg and C. Granqvist, *J. Appl. Phys.* **60,** R123 (1986).
3. R. Wang, A. Sleight, R. Platzer, and J. A. Gardner, *J. Mater. Res.* **11,** 1659 (1996).
4. T. Minami, T. Kakumu, and S. Takata, *J. Vac. Sci. Technol. A.* **14,** 1704 (1996).
5. J. M. Phillips, R. J. Cava, G. A. Thomas, S. A. Carter, J. Kwo, T. Siegrist, J. Krajewski, J. Marshall, W. Peck, and D. Rapkine, *Appl. Phys. Lett.* **67,** 2246 (1995).
6. T. Moriga, D. Edwards, T. Mason, G. Palmer, K. Poeppelmeier, J. Schindler, and C. Kannewurf, *J. Am. Ceram. Soc.* [in press].
7. H. Enoki, T. Nakayama, and J. Echiyoga, *Phys. Status Solidi* **129**, 181 (1992).
8. H. Enoki, T. Nakayama, and J. Echiyoga, *Phys. Status Solidi* **137**, 135 (1993).
9. T. Minami, S. Takata, and H. Sonohara, *J. Vac. Sci. Technol.* **13,** 1095 (1995).
10. G. Palmer, K. Poeppelmeier, and T. Mason, *Chem. Mater.* [in press]
11. T. Barth and E. Posnjak, *Z. Kristallogr.* **82,** 325 (1932).
12. P. Georgopoulos, "XRAYFIT", Fortran program. Northwestern University, Evanston, IL, 1993.
13. D. Keszler, D. Cahen, and J. Ibers, "POLSQ", Fortran program. Northwestern University, Evanston, IL, 1984.
14. F. M. Smits, *Bell Syst. Tech. J.* **37,** 711 (1958).
15. H. Hecht, "Modern Aspects of Reflectance Spectroscopy" (W. Wendlandt, Ed.), pp. 1–22. Plenum Press, New York, 1968.
16. R. D. Shannon, *Acta Crystallogr. A* **32,** 751 (1976).
17. R. Tyson and L. Chang, *J. Am. Ceram. Soc.* **64,** C4 (1981).
18. M. Nakamura, N. Kimizuka, and T. Mohri, *J. Solid State Chem.* **86,** 16 (1990).
19. H. Kasper, *Z. Anorg. Allg. Chem.* **349,** 113 (1967).
20. P. Cannard and R. Tilley, *J. Solid State Chem.* **73,** 418 (1988).
21. J. Choisnet, A. Deschanvres, and B. Raveau, *C. R. Acad. Sci. Paris. C* **266,** 543 (1968).
22. J. Rodriguez-Carvajal, "FULLPROF," Ver. 3.1-c, Fortran program. Laboratoire Leon Brillouin (CEA–CNRS), Saclay, France, Jan. 1996.
23. E. Burstein, *Phys. Rev.* **93,** 632 (1954).